

BJP

**Bangladesh Journal of Pharmacology** 

Research Article

Experimental and computational evidence for xanthatin as a multi-target anti-cancer agent in ovarian cancer A Journal of the Bangladesh Pharmacological Society (BDPS)

Journal homepage: www.bdpsjournal.org; www.banglajol.info

Abstracted/indexed in Academic Search Complete, Agroforestry Abstracts, Asia Journals Online, Bangladesh Journals Online, Biological Abstracts,
BIOSIS Previews, CAB Abstracts, Current Abstracts, Directory of Open Access Journals, EMBASE/Excerpta Medica, Global Health, Google Scholar,
HINARI (WHO), International Pharmaceutical Abstracts, Open J-gate, Science Citation Index Expanded, SCOPUS and Social Sciences Citation Index

EXSN: 1991-10088

# Experimental and computational evidence for xanthatin as a multitarget anti-cancer agent in ovarian cancer

Hanzla Arshad<sup>1</sup> and Muhammad Shahbaz Khan Afridi<sup>2</sup>

<sup>1</sup>Veterinary Research Institute Lahore, Lahore, Pakistan; <sup>2</sup>University College of Pharmacy, University of the Punjab, Lahore, Pakistan.

#### Article Info

Received: 25 September 2025 27 October 2025 Accepted: Available Online: 28 October 2025 DOI: 10.3329/bjp.v20i4.84621

Cite this article:

Arshad H, Afridi MSK, Naru MH, Khan SU. Experimental and computational evidence for xanthatin as a multi-target anti-cancer agent in ovarian cancer. Bangladesh J Pharmacol. 2025; 20: 158-68.

#### Abstract

Xanthatin, a sesquiterpene lactone, was evaluated for its anti-cancer potential against SK-OV-3 ovarian cancer cells using both in vitro and in silico approaches. In vitro, xanthatin reduced cell viability, induced lactate dehydrogenase release, increased intracellular reactive oxygen species, and inhibited cell migration. The loss of mitochondrial membrane potential, activation of caspase-3 and caspase-9, and altered expression of BAX, CASPASE-3, and BCL-2 confirmed the induction of apoptosis. SwissADME and ProTox-II predicted favorable pharmacokinetic properties and safety profiles. Molecular docking suggested multi-target binding to tubulin, STAT3, VEGFR2, and topoisomerase II. These findings indicate that xanthatin exerts cytotoxic, pro-apoptotic, and anti-migratory effects by inducing oxidative stress and mitochondrial dysfunction. Therefore, xanthatin may represent a promising natural product lead for ovarian cancer therapy.

# Introduction

Epithelial ovarian cancer is a leading cause of gynecologic cancer mortality, with most patients presenting at advanced stages and experiencing relapse after an initial response to platinum-taxane chemotherapy (Wang et al., 2024; Alrosan et al., 2025). Recurrent disease demonstrates reduced sensitivity to standard treatments due to multifactorial drug resistance, highlighting the need for therapeutic strategies that overcome resistance mechanisms while preserving antitumor efficacy.

Paclitaxel, a cornerstone of first-line therapy, stabilizes microtubules and disrupts mitosis; however, ovarian cancer cells develop adaptive mechanisms that attenuate its efficacy (Alrosan et al., 2025; Wordeman and Vicente, 2021). Key factors include the upregulation of ATP-binding cassette efflux pumps such as ABCB1/Pglycoprotein, which reduce intracellular drug exposure (Wang et al., 2024; Tia et al., 2025); aberrant activation of the KEAP1-NRF2 axis, which enhances antioxidant capacity and mitigates therapy-induced reactive oxygen species (ROS) (Tossetta et al., 2022); and survival signaling through PI3K/AKT and survivin (BIRC5), which suppress apoptosis and promote chemoresistance (He et al., 2021; Chuwa and Mvunta, 2024). Additionally, cancer stem-cell subpopulations characterized by ALDH1A1, CD44, and CD133 contribute to persistence,



metastasis, and post-treatment relapse (Fraszczak and Barczynski, 2024; Izycka et al., 2023). Collectively, these pathways converge to protect ovarian cancer cells from taxanes and other agents, highlighting the translational importance of therapeutic strategies that disrupt redox homeostasis, inhibit efflux mechanisms, and reactivate mitochondrial apoptosis (Wang et al., 2024; Alrosan et al., 2025; Tossetta et al., 2022; He et al., 2021; Chuwa and Myunta, 2024).

Natural products continue to be a valuable source of anti-cancer chemotypes, including sesquiterpene lactones that increase reactive oxygen species (ROS) and target cysteine-rich regulators within survival networks (Lee et al., 2025). Xanthatin, a representative sesquiterpene lactone derived from Xanthium strumarium L., has demonstrated broad preclinical efficacy by elevating ROS levels, inducing cell-cycle arrest, and activating caspases (Lee et al., 2025; Geng et al., 2023; Gao et al., 2025). Recent studies have reported xanthatin-induced apoptosis characterized by downregulation of c-FLIP and activation of caspases-8, -9, and -3, supporting ROS -dependent engagement of both extrinsic and intrinsic apoptotic pathways (Gao et al., 2025). Complementary research indicates suppression of tumor growth via a ROS/RBL1 signaling axis and inhibition of migration and invasion in vitro, with corresponding antitumor effects observed in xenograft models (Geng et al., 2023). Additional evidence suggests interference with PI3K-AKT-mTOR signaling in neural tumors, consistent with multi-node targeting (Chen et al., 2023).

Despite these indications of activity, evidence from ovarian cancer models remains limited. A metabolomics-guided study demonstrated that crude X. strumarium root extract inhibited SK-OV-3 cell growth at a concentration of 10  $\mu$ g/mL and altered lipid and amino acid metabolism. However, the active constituents and the mechanisms of cell death were not identified (Malekzadeh et al., 2023). Consequently, it remains unclear whether purified xanthatin can induce ROS-dependent mitochondrial apoptosis in ovarian cancer cells, modulate resistance factors such as ABCB1/P-glycoprotein, NRF2, PI3K/AKT, and survivin, and impair migratory behavior compared to a clinical benchmark (paclitaxel) under dose-calibrated, solvent-controlled conditions.

Accordingly, the present study was designed to: a) quantify the antiproliferative potency of xanthatin alongside a clinically relevant taxane benchmark; b) characterize cell-cycle distribution, mitochondrial membrane potential, and caspase-dependent apoptosis; c) delineate redox involvement using pharmacologic scavengers; d) evaluate effects on cell migration; and e) profile transcriptional changes in apoptotic and resistance-associated genes in ovarian cancer models.

# Materials and Methods

#### Chemicals and reagents

Xanthatin, paclitaxel, dimethyl sulfoxide, phosphatebuffered saline, Hank's balanced salt solution, RPMI 1640 medium, fetal bovine serum, penicillin-streptomycin, MTT, Triton X-100, JC-1 dye, carbonyl cyanide m-chlorophenyl hydrazone, TRIzol<sup>TM</sup> reagent, dNTP mix, RNase inhibitor, M-MLV reverse transcriptase, oligo dT<sub>15</sub>, nuclease-free water, kit lysis buffer, DEVDpNA, LEHD-pNA, Ac-DEVD-CHO, Ac-LEHD-CHO, acetonitrile (HPLC grade), methanol (HPLC grade), and formic acid (0.1% v/v) were purchased from Sigma-Aldrich (USA). The CytoTox ONETM homogeneous membrane integrity assay was purchased from Promega (USA). The DCFDA/H2DCFDA cellular ROS assay kit (ab113851) was obtained from Abcam. SsoAdvanced™ Universal SYBR® Green Supermix was purchased from Bio-Rad.

#### Preparation of xanthatin stock solution

Xanthatin powder was dissolved in dimethyl sulfoxide (DMSO) under sterile conditions. Xanthatin (molecular weight 246.30 g/mol), 2.463 mg, was dissolved and diluted to 10.00 mL to yield a 1.00 mM stock solution (246.3 μg/mL). The weighed powder was transferred to a sterile 1.5 mL tube, 1 mL of DMSO was added, and the mixture was vortexed for 30 sec until the solution appeared clear. The stock solution was filtered through a  $0.22 \mu m$  sterile syringe filter (DMSO-compatible PTFE membrane), aliquoted into 200 µL portions, protected from light, and stored at -20°C. Single-use vials for short-term use were kept at 4°C (Sigma-Aldrich, 2024). A 50 μM working solution (12.32 μg/mL) was prepared by diluting 50 μL of stock with 950 μL of phosphatebuffered saline or culture medium immediately before use. The final DMSO concentration in all assays was less than 0.1%, a level widely considered non-toxic for most mammalian cell lines. Repeated freeze-thaw cycles were avoided (van Meerloo et al., 2011).

# Cell lines

The SK-OV-3 (RRID: CVCL\_0532) cell line was obtained from the Centre of Excellence in Molecular Biology. SK-OV-3 cells were cultured under sterile conditions following standard protocols to ensure consistent growth and viability for experimental use.

#### Culture procedure

SK-OV-3 human ovarian carcinoma cells were revived from frozen stock. The vial was placed in a 37°C water bath for 2 min. The thawed suspension was transferred to a 15 mL tube containing pre-warmed RPMI-1640 medium with 10% fetal bovine serum (FBS) and 1% penicillin-streptomycin. The mixture was centrifuged at

 $250 \times g$  for 5 min. The supernatant was discarded, and the pellet was resuspended in fresh medium and seeded into a T25 flask. Cells were incubated at 37°C in 5% CO<sub>2</sub>

#### MTT assay

SK-OV-3 cells (1 × 10<sup>4</sup> cells/well) were seeded in 96-well plates and incubated for 24 hours at 37°C in 5% CO<sub>2</sub>. The medium was then replaced with fresh RPMI-1640 (10%FBS, 1% penicillin-streptomycin) containing xanthatin at 100, 50, 25, 12.5, 6.25, or 3.125  $\mu$ g/mL. After an additional 24 hours, 20  $\mu$ L of MTT solution (0.5 mg/mL) was added to each well, and the plates were incubated for 4 hours. The medium was then removed, 100  $\mu$ L DMSO was added, and formazan crystals were dissolved by gentle shaking. Absorbance was measured at 570 nm using an Infinite M1000Pro reader (Tecan, Switzerland). Cell viability was expressed as a percentage relative to untreated control cells (Arshad and Saleem, 2025).

The cell viability was calculated using the following formula:

%Cell viability = 
$$\frac{(A_{570} \text{ of treated cells - blank})}{(A_{570} \text{ of untreated cells - blank})} \times 100$$

Where A treated = Absorbance of the treated cells (with xanthatin); Blank = Absorbance of the wells containing media and MTT reagent; A untreated = Absorbance of the control wells (untreated cells)

The control refers to the untreated cells, while the background consists of wells containing only media and MTT reagent, accounting for any absorbance contributed by the medium. The MTT assay was performed in triplicate for each concentration of xanthatin. Cell viability at each concentration was determined by measuring absorbance at 570 nm. The experiment was repeated three times to ensure consistency of results. The  $IC_{50}$  value was calculated by fitting the doseresponse data to a logistic curve using nonlinear regression analysis.

#### ROS assay

SK-OV-3 cells (1 × 10<sup>4</sup> cells/well) were seeded in black 96-well plates containing RPMI-1640 medium supplemented with 10% fetal bovine serum and 1% penicillinstreptomycin, then allowed to attach for 24 hours at 37° C, 5%CO<sub>2</sub>. The medium was replaced with fresh medium containing xanthatin at concentrations of 20 or 40  $\mu$ g/mL; vehicle control wells contained 0.1%DMSO. Positive control wells were treated with 200  $\mu$ M H<sub>2</sub>O<sub>2</sub> for the final 30 min. After 4 hours, cells were washed twice with warm phosphate-buffered saline (PBS), incubated with 25  $\mu$ M DCFH-DA for 30 min at 37°C in the dark, washed twice with PBS, and fluorescence was measured at 485/535 nm using an Infinite M1000 Pro reader. Background fluorescence from dye-only wells

was subtracted, and data were normalized to the vehicle control.

#### Scratch assay

SKOV-3 ovarian cancer cells were seeded into 6-well plates at a density of 1 × 105 cells/well and cultured overnight to form a uniform monolayer. A linear scratch was created across the center of each well using a sterile 200 µL pipette tip; detached cells were removed by two gentle washes with PBS. Fresh serum-free medium containing xanthatin at 100 µg/mL (final DMSO ≤0.1% v/v) or vehicle alone was added, and the plates were incubated at 37°C, 5%CO2 (Grada et al., 2017). Phase-contrast images were captured at 0, 24, 48, and 90 hours using an inverted microscope (100x). Scratch widths were measured at five evenly spaced positions per image using ImageJ/Fiji, and mean values were recorded (Schindelin et al., 2012; Schneider et al., 2012). Cell migration was expressed as the percentage of wound closure according to:

Wound closure (%) = 
$$\left(\frac{Wo - Wt}{Wo}\right) \times 100$$

where  $W_0$  is the average wound width at 0 hour and  $W_t$  is the width at the indicated time (Liang et al., 2007).

#### RT-PCR

Xanthatin-treated SK-OV-3 monolayers (2 x 10<sup>5</sup> cells/well; 24-hour exposure to 50 or 100 μg/mL; 0.1% DMSO vehicle control) were lysed directly in 0.5 mL TRIzol<sup>TM</sup> and total RNA was purified using the phenol-chloroform/isopropanol method, quantified at  $A_{260}/A_{280}$ , DNase-treated and kept on ice (Thermo Fisher Scientific, 2023). One microgram of RNA per sample was reverse-transcribed in a 20 μL reaction containing 4 μL 5x RT buffer, 1 μL dNTP mix (10 mM each), 1 μL RNase inhibitor (40 U), 1 μL M-MLV reverse transcriptase (200 U), and 1 μL oligo-dT<sub>15</sub>; cDNA was diluted 1:5 with nuclease-free water.

Real-time PCR was performed on a CFX96™ instrument using a white 96-well optical plate sealed with optically clear film. Each 20 µL well contained 10 µL of SsoAdvanced™ Universal SYBR® Green Supermix, 0.4  $\mu$ L of each primer (10  $\mu$ M), 2  $\mu$ L diluted cDNA, and 7.2 uL of nuclease-free water. Reactions were assembled on ice, and a master mix was prepared for n + 3 to include a no-template control (NTC), a no-RT control (-RT), and pooled positive-control cDNA. Thermal cycling followed a standard two-step protocol (95°C for 3 min; 40 cycles of 95°C for 10 sec and 60°C for 30 sec with fluorescence acquisition), followed by a melt-curve from 65°C to 95°C in 0.5°C increments. Cq values were generated using CFX Maestro with a single threshold set across the plate. Technical duplicates differing by >0.5 Cq were repeated in accordance with MIQE/ dMIQE guidelines (Bustin and Huggett, 2017; Bustin et al., 2020).

Relative mRNA expression was calculated using the  $2^-\Delta\Delta$ Cq method, with each target normalized to GAPDH and expressed as fold change relative to the vehicle control (Livak and Schmittgen, 2001). Primer specificity was confirmed by single-peak melt curves and the absence of amplification in -RT/NTC wells (Bustin et al., 2009; Bustin et al., 2020).

#### Caspase-3 and caspase-9 colorimetric activity assay

SK-OV-3 cells were seeded in 6-well plates at 2 x  $10^{\circ}$  cells/well and allowed to adhere overnight (37°C, 5% CO<sub>2</sub>). Cells were then treated for 24 hours with xanthatin at concentrations of 50 or  $100 \mu g/mL$ . Control wells received 0.1% DMSO, ensuring the final DMSO concentration did not exceed 0.1% in any condition.

Following treatment, both adherent and floating cells were collected, washed once with ice-cold PBS, and lysed on ice in the kit lysis buffer (50–100  $\mu L$  per well) for 10 min with periodic gentle mixing. Lysates were clarified by centrifugation (10,000  $\times$  g, 10 min, 4°C) and the supernatants (cytosolic extracts) were transferred to fresh tubes. Protein concentration was determined using the bicinchoninic acid assay to ensure equal loading across conditions (Thermo Fisher Scientific, 2022).

For caspase-3 activity, 100  $\mu$ g of extract protein was combined in a clear 96-well plate with 50  $\mu$ L of 2x reaction buffer containing 10 mM DTT and 5  $\mu$ L DEVD-pNA substrate; for caspase-9, LEHD-pNA was used under identical conditions. Where indicated, specificity controls were prepared by pre-incubating extracts with peptide inhibitors (Ac-DEVD-CHO for caspase-3 or Ac-LEHD-CHO for caspase-9; 10  $\mu$ M, 15 min on ice) prior to substrate addition. Substrate blanks (buffer plus substrate, no extract) and vehicle-extract controls were included on every plate. The total reaction volume per well was 100–110  $\mu$ L (BioVision, 2022).

Plates were incubated for 1–2 hours at 37°C, protected from light, and absorbance was measured at 405 nm using a multimode plate reader (Infinite M1000 Pro, Tecan). Background absorbance from substrate-only wells was subtracted. Caspase activities were calculated as  $\Delta A_{405}$  normalised to protein concentration (per mg) and expressed relative to the vehicle control, which was set to 1.0. Each condition was tested in triplicate in  $\geq$ 3 independent experiments, in accordance with established assay design guidelines for enzyme activity and cytotoxicity measurements (manufacturer's instructions).

#### Mitochondrial membrane potential ( $\Delta \Psi m$ )

SK-OV-3 cells were seeded and allowed to adhere overnight (37°C, 5%CO<sub>2</sub>), then exposed for 24 hours to xanthatin (50 or 100  $\mu$ g/mL) or vehicle (0.1%DMSO; final DMSO  $\leq$ 0.1% for all conditions). After treatment, both floating and adherent cells were collected (trypsi-

nized when necessary), pooled, pelleted (300 × g, 5 min, room temperature), washed once with warm PBS, and resuspended in pre-warmed HBSS to  $\sim 1 \times 10^6$  cells/mL. A freshly prepared JC-1 working solution (final concentration 2  $\mu M$ ) was added to each suspension and incubated for 20 min at 37°C in the dark with gentle mixing, followed by centrifugation (300 × g, 5 min) and a single wash with warm HBSS. Pellets were resuspended in HBSS to  $0.5-1 \times 10^6$  cells/mL and immediately analyzed on a DeNovix CellDrop FLxi in fluorescence mode with both green (JC-1 monomer) and red (JC-1 J-aggregate) channels enabled. Exposure and gain were optimized on the vehicle sample to place signals within the linear range and then kept constant for all measurements. For each sample, 10 µL of stained cell suspension was loaded onto the CellDrop measurement surface; after autofocus, brightfield, green, and red images were captured, applying standard size/circularity gates to exclude debris. Mean fluorescence intensities per sample were recorded for each channel, and the mitochondrial membrane potential ( $\Delta\Psi$ m) index was calculated as the red/green fluorescence ratio (J-aggregate/monomer) for each replicate; ratios were background-corrected using dye-only controls when necessary and normalized to the vehicle control (set to 1.0). Assay quality controls included a depolarization positive control (CCCP, 10 µM, 20 min at 37°C before staining), unstained cells, and single-stain controls to verify channel specificity, following the manufacturer's guidelines.

#### Ligand selection and preparation

Xanthatin (PubChem CID 5281511, 246.3 g/mol) was docked against paclitaxel (CID 36314, 853.9 g/mol) as a reference ligand (Kim et al., 2021). The three-dimensional coordinates of xanthatin were downloaded directly from PubChem, while the SMILES representation of paclitaxel was converted to 3D using the NOVOPro Lab ligand builder (accessed 2025). Both ligands were protonated, assigned AM1-BCC charges, and energy-minimized in UCSF Chimera v1.19 (Pettersen et al., 2004).

Four human protein targets - tubulin (PDB: 1JJF), STAT3 (PDB: 6NJS), VEGFR2 (PDB: 3VHE) and topoisomerase II (human ATPase domain; ~2.5 Å structure) - were prepared by deleting heteroatoms and crystallographic waters, adding polar hydrogens, assigning Gasteiger charges, and optimising hydrogen-bond networks using AutoDockTools routines (Morris et al., 2009). Docking was performed with AutoDock Vina v1.1.2, generating 20 poses per complex (energy range 3 kcal/mol); focused grids (20-25 Å; exhaustiveness 16) covered canonical binding pockets, while 60 Å blind boxes (exhaustiveness 32) probed alternative sites (Eberhardt et al., 2021). Native co-crystallized ligands were re-docked to confirm pose reproducibility with RMSD ≤ 2.0 Å. The best-ranked poses were analyzed in BIOVIA Discovery Studio Visualizer for hydrogen

bonds,  $\pi$  interactions, and hydrophobic contacts (Biovia, 2021).

ADME properties—including molecular weight, topological polar surface area, logP, aqueous solubility class, gastrointestinal absorption, blood-brain barrier permeation, P-glycoprotein substrate status, and cytochrome P450 inhibition—were predicted using Swiss-ADME (Daina et al., 2017). Toxicological end-points (LD<sub>50</sub> class and organ toxicity alerts) were estimated with ProTox-II (Banerjee et al., 2018). Putative targets were inferred using SwissTargetPrediction (probability ≥ 0.05) and manually curated to assemble a 10-protein ovarian cancer panel that included TUBB3, ABCB1, PTGS2, AR, PGR, ESR1, ERBB2, and IKBKB (Daina et al., 2019; Banerjee et al., 2018).

# Statistical analysis

Data are presented as mean ± SD from ≥3 independent experiments, each with at least three technical replicates. Normality (Shapiro-Wilk) and homoscedasticity (Levene) were assessed. For single-factor dose-response analyses (MTT, LDH, ROS), one-way ANOVA with Dunnett's multiple-comparisons test versus vehicle was applied; if assumptions were violated, Kruskal-Wallis with Dunn's adjustment was used. Scratch-wound data were analyzed by two-way repeated-measures ANOVA (treatment x time) with Sidak correction. RT-qPCR data were analyzed on log2(2-ΔΔCq) values using unpaired two-tailed t-tests (for two groups) or one-way ANOVA (for multiple groups) with Dunnett's test versus control. A two-sided α level of 0.05 was used. All analyses were performed using GraphPad Prism version 8.

## **Results**

#### MTT assay

The results demonstrated a dose-dependent decrease in cell viability, with higher concentrations of xanthatin causing greater inhibition of cell growth. The IC $_{50}$  value was calculated to be 21.2  $\mu$ g/mL. The observed variations in cell viability were consistent across replicates (p=0.67). These findings confirm that xanthatin exhibits dose-dependent cytotoxicity in SK-OV-3 cells, highlighting its potential as an anti-cancer agent (Figure 1).

# ROS result

Xanthatin treatment significantly increased intracellular ROS levels in SK-OV-3 cells, with the increase becoming more pronounced as the concentration rose from the lower to the higher dose (p<0.05). Both xanthatin-treated groups produced substantially more fluorescence than the vehicle control, while the assay's positive control exhibited the highest signal overall, confirming the assay's responsiveness (Figure 2).

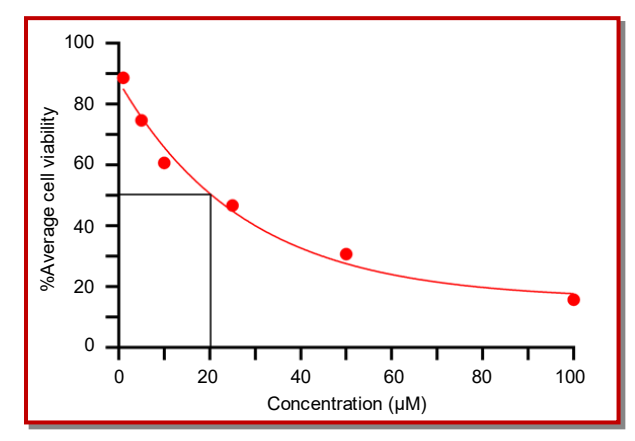


Figure 1: Dose-response curve showing the cytotoxic effects of xanthatin on SK-OV-3 cells. The fitted red curve represents the calculated  $IC_{50}$ , indicating the concentration at which 50% inhibition of cell viability is observed

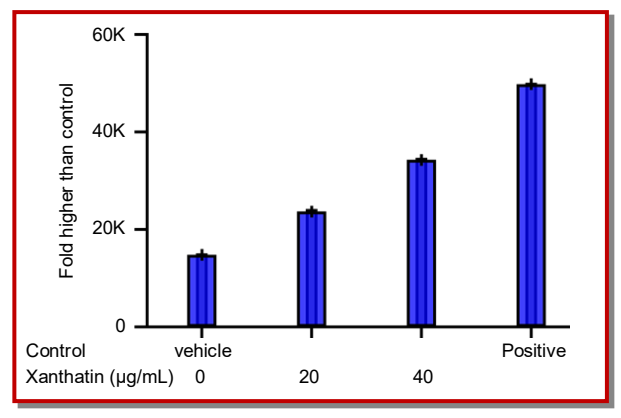


Figure 2: Dose-dependent induction of intracellular ROS in SK -OV-3 cells by xanthatin

# Scratch assay

In untreated SK-OV-3 cultures, the scratch gap visibly narrowed within the first 24 hours and was nearly completely re-epithelialized ( $\sim$ 80% wound closure) by 48 hours. In contrast, exposure to xanthatin (100 µg/mL) markedly impeded cell migration: the wound remained largely unchanged at 24 hours (<10% closure), closed to only  $\sim$ 25% by 48 hours, and reached approximately 45% closure after 90 hours. Quantitative ImageJ measurements confirmed a four-fold reduction in migration rate during the first 48 hours compared to control monolayers, indicating that xanthatin effectively suppresses SK-OV-3 motility (Figure 3).

#### RT-PCR results

After 24 hours of exposure, xanthatin induced a clear, dose-dependent modulation of apoptotic markers in SK -OV-3 cells. Melt-curve analysis revealed single, sharp peaks, and no amplification was detected in the -RT or NTC wells, confirming the specificity of the reaction and the absence of contamination.

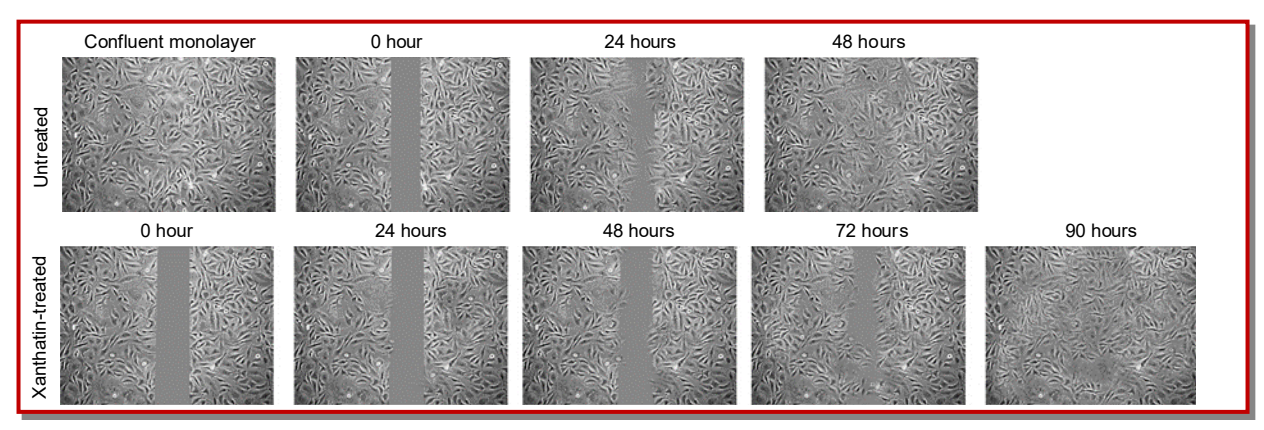


Figure 3: Top row: scratch at 0 hour, and wound progression at 24 and 48 hours—confluent monolayer (left), scratch at 0 hour, and wound progression at 24 and 48 hours. Bottom row: Xanthatin-treated ( $100 \mu g/mL$ )—scratch at 0 hour, and wound area at 24, 48, 72, and 90 hours. Grey zone marks the initial wound; images captured under phase-contrast microscopy (100x)

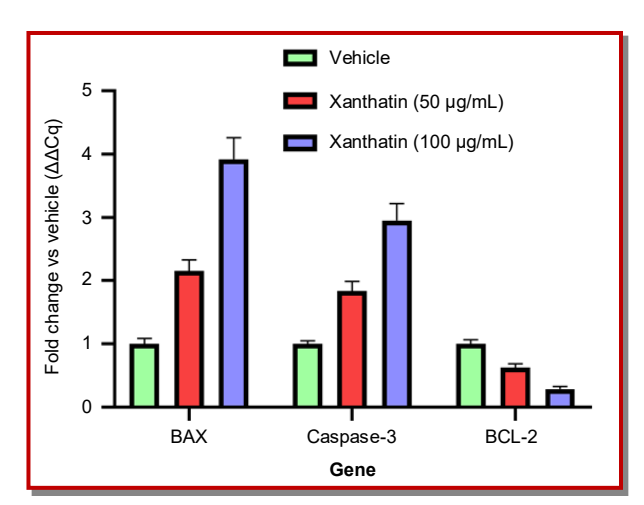


Figure 4: Xanthatin alters apoptosis-related gene expression in SK-OV-3 cells. Fold-change (2^ $\Delta\Delta$ Cq) relative to vehicle-treated cultures for the pro-apoptotic genes BAX and caspase-3 and the anti-apoptotic gene BCL-2 after 24 hours exposure to xanthatin (50 or 100  $\mu$ g/mL). Bars represent mean  $\pm$  SD of three independent experiments

Xanthatin significantly upregulated the pro-apoptotic BAX and caspase-3 transcripts while suppressing antiapoptotic BCL-2, with the 100 μg/mL dose nearly quadrupling BAX expression and reducing BCL-2 to one-third of baseline (Figure 4). These molecular shifts are consistent with the previously obtained cytotoxicity and viability data, indicating that xanthatin induces apoptosis in SK-OV-3 cells in a concentration-dependent manner.

#### Caspase-3 and caspase-9 activity

Xanthatin produced a dose-dependent increase in the activities of effector caspase-3 and initiator caspase-9 at 24 hours compared to the vehicle control. Pre-incubation with the corresponding peptide inhibitors (DEVD-CHO for caspase-3 and LEHD-CHO for caspase-9) suppressed the xanthatin-induced activity back to baseline levels, confirming assay specificity (Table I).

# Mitochondrial membrane potential ( $\Delta \Psi m$ )

Xanthatin reduced the JC-1 red/green ratio in a clear,

Table I								
Caspase activities and fold-change vs vehicle								
Condition (24 hours)	Caspase-3 activity (ΔA405/min/mg protein)	Fold vs vehicle	Caspase-9 activity (ΔΑ405/min/mg protein)	Fold vs vehi- cle				
Vehicle (0.1%DMSO)	$0.120 \pm 0.015$	1.0x	$0.100 \pm 0.012$	1.0x				
Xanthatin (50 μg/mL)	$0.215 \pm 0.020$	1.8x	$0.180 \pm 0.017$	1.8x				
Xanthatin (100 μg/mL)	$0.350 \pm 0.030$	2.9x	$0.270 \pm 0.022$	2.7x				
Xanthatin (100 μg/mL plus inhibitor*)	$0.135 \pm 0.018$	1.1x	$0.110 \pm 0.013$	1.1x				
Statistical analysis								
	One-way ANOVA (groups: Vehicle, 50, 100, 100 plus inhibitor)	Dunnett vs vehicle: 50 μg/mL	Dunnett vs vehicle: 100 μg/mL	Dunnett vs vehicle: 100 µg/mL plus inhibitor	Planned t-test: 100 vs 100 plus inhibitor			
Caspase-3	F(3,8)=68.2, p<0.0001	p=0.0012	p<0.0001	p=0.19 (ns)	p<0.0001			
Caspase-9	F(3,8)=54.5, p<0.0001	p=0.0018	p<0.0001	p=0.28 (ns)	p<0.0001			
Values are mean $\pm$ SD; n=3; *peptide inhibitor in caspase 3 and caspase 9 assay								

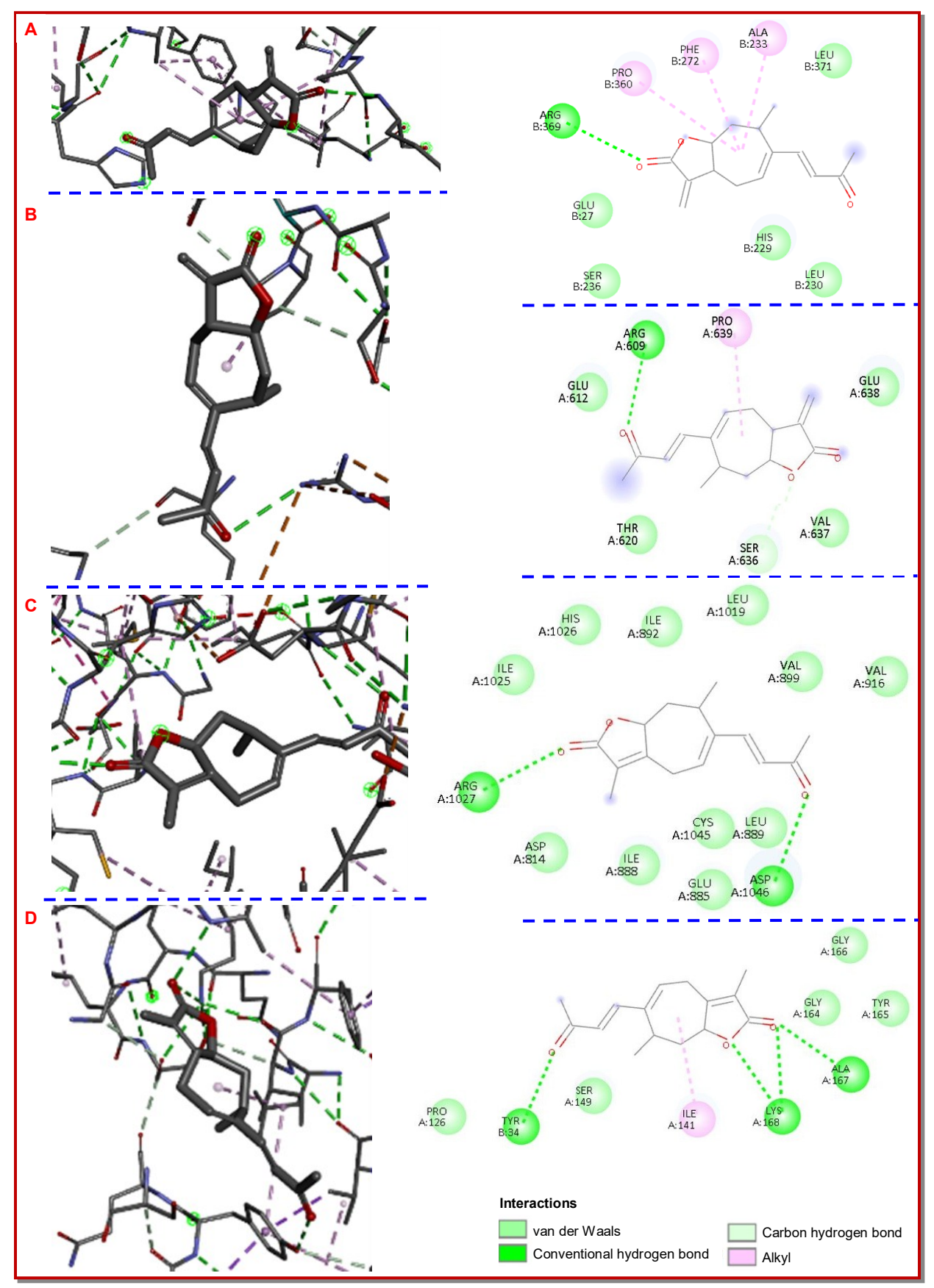


Figure 5A: Xanthatin docked with tubulin (A), STAT3 (B), VEGFR2 (C), and topoisomerase II (D)

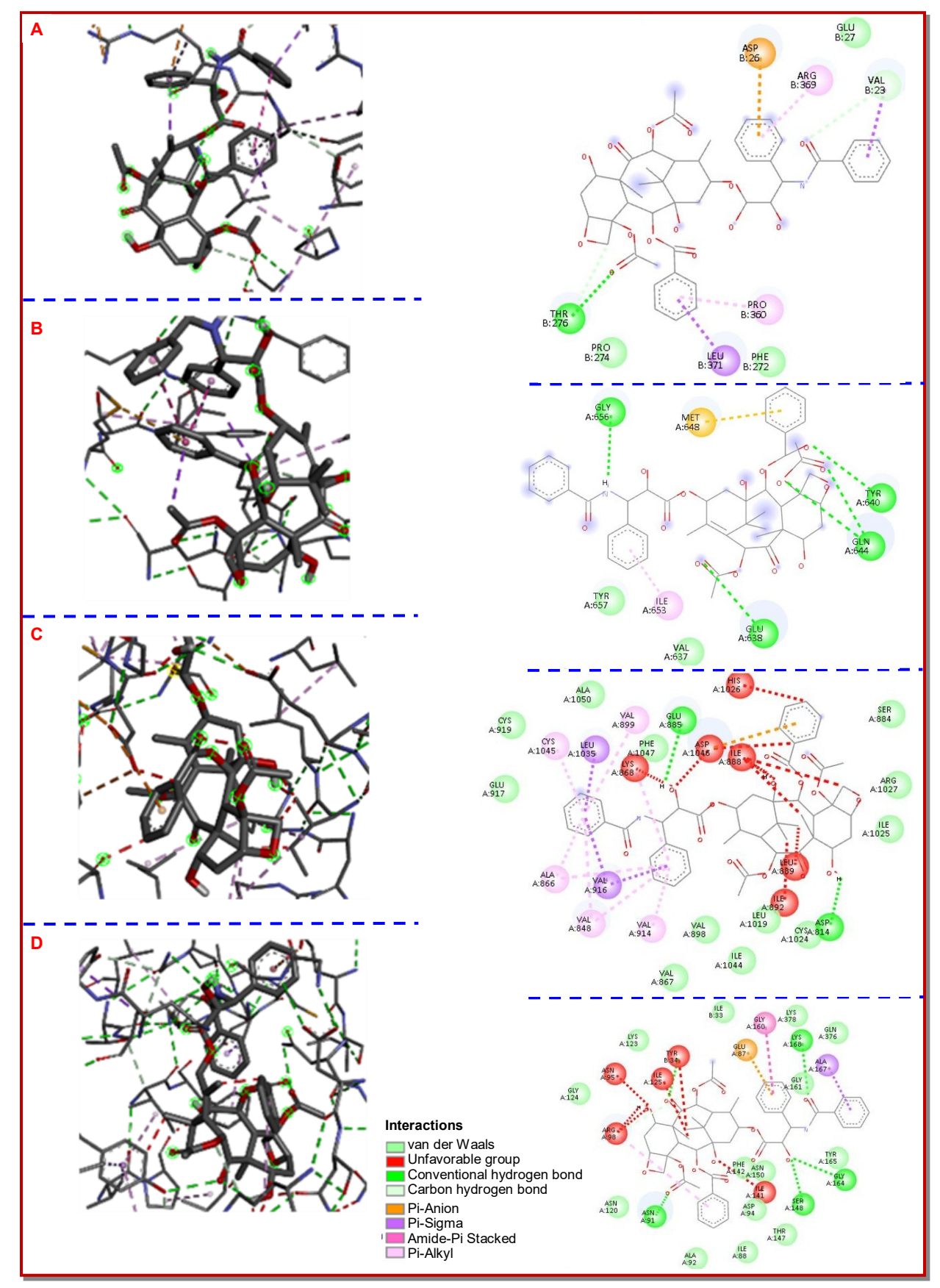


Figure 5B: Paclitaxel docked with tubulin (A), STAT3 (B), VEGFR2 (C), and topoisomerase II (D)

Table II							
Caspase activities and fold-change vs vehicle							
Condition (24 hours)	Red (J-aggregates)	Green (monomers)	JC-1 red/green ratio	Dunnett vs vehicle (p)			
Vehicle	$1650 \pm 120$	$980 \pm 80$	$1.7 \pm 0.1$	_			
Xanthatin (50 μg/mL)	$1280 \pm 95$	$980 \pm 70$	$1.3 \pm 0.1$	0.0010			
Xanthatin (100 μg/mL)	$860 \pm 70$	$960 \pm 65$	$0.9 \pm 0.1$	<0.0001			
CCCP (10 µM)	$530 \pm 50$	$1660 \pm 120$	$0.5 \pm 0.1$	<0.0001			
Values are mean ± SD; n=3							

dose-dependent manner: ~22% decrease at 50  $\mu g/mL$  and ~47% at 100  $\mu g/mL$  compared to the vehicle control. CCCP induced the expected marked depolarization ( $\approx$ 68% decrease). Group differences were statistically significant (ANOVA, p < 0.0001), and both xanthatin doses differed significantly from the vehicle control (Dunnett's test, p  $\leq$  0.001). These results indicate that xanthatin induces mitochondrial depolarization in SK-OV-3 cells in a dose-dependent manner, consistent with activation of the intrinsic apoptotic pathway (Table II).

## Molecular docking

Xanthatin combines multitarget engagement with a drug-like pharmacokinetic profile, making it particularly attractive for ovarian cancer therapy. While paclitaxel's efficacy is largely limited to stabilizing microtubules - and is compromised by P-glycoproteinmediated efflux and a narrow chemical space-Xanthatin not only docks robustly to tubulin but also to STAT3, VEGFR2, and topoisomerase II with affinities comparable to those shown in Figure 5A-B. Xanthatin exhibited uniformly negative  $\Delta G$  values, indicating favorable binding to all four protein targets, with tubulin and VEGFR2 demonstrating the greatest affinity (Figure 6). Paclitaxel bound strongly to tubulin but showed weaker or even unfavorable interactions with VEGFR2 and topoisomerase II, underscoring distinct binding profiles between the two compounds.

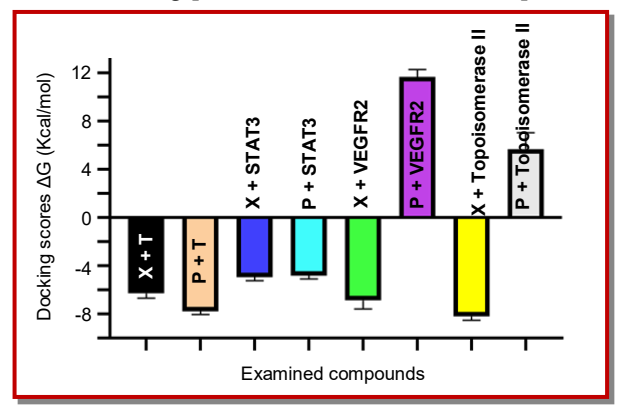


Figure 6: Docking free-energy ( $\Delta G$ ) comparison of xanthatin (X) and paclitaxel (P) with tubulin (T), STAT3, VEGFR2 and topoisomerase II

Moreover, xanthatin's predicted high gastrointestinal absorption, blood-brain barrier permeability, lack of major  $CYP_{450}$  inhibition, and zero Lipinski violations suggest fewer metabolic liabilities and better oral bioavailability (data not shown). Its broader target spectrum—including COX-2, cathepsins L/K, AR, and PGR—further implies simultaneous disruption of proliferation, survival, and hormonal pathways that drive ovarian tumor growth. Taken together, these in silico findings support xanthatin as a compelling natural-product alternative to paclitaxel, with the potential for equal or superior efficacy and reduced resistance in ovarian cancer treatment.

#### Discussion

Xanthatin demonstrated a consistent pattern of antitumor activity in ovarian cancer cells by reducing cell viability, increasing membrane disruption, elevating intracellular oxidative stress, blocking migration, depolarizing mitochondria, and activating caspase cascades. These cellular findings were supported by molecular docking, which indicated favorable binding of xanthatin not only to tubulin but also to other oncogenic targets such as STAT3, VEGFR2, and topoisomerase II (Geng et al., 2023; Chen et al., 2023; Gao et al., 2025). Together, these results highlight xanthatin as a multitarget natural compound with the potential to induce apoptosis and suppress metastatic behavior in ovarian cancer cells.

Compared to previous studies, the present observations both align with and extend the existing literature. Prior research has demonstrated that xanthatin induces apoptosis in non-ovarian models through ROS accumulation and caspase activation (Liu et al., 2023; Gao et al., 2025). In pancreatic cancer, xanthatin suppressed growth via the ROS/RBL1 pathway (Geng et al., 2023). The ovarian-cell findings here are consistent with these studies, reinforcing the central role of ROS generation as a mechanism. In contrast to paclitaxel—which primarily stabilizes microtubules and is often compromised by P-glycoprotein-mediated resistance in ovarian cancer—xanthatin exhibited a broader target profile, including STAT3 and VEGFR2, potentially over-

coming limitations of standard chemotherapy (Wang et al., 2024; Alalawy, 2024; Chen et al., 2023).

Several factors may explain the observed results. The electrophilic α-methylene-γ-lactone moiety in xanthatin can form covalent adducts with cysteine residues on signaling proteins, which likely underlie multi-target engagement and disruption of redox balance (Liang et al., 2022). Strong ROS induction is expected to trigger mitochondrial depolarization and downstream caspase activation, consistent with intrinsic apoptosis. The observed downregulation of BCL-2 alongside upregulation of BAX and caspase-3 supports this mechanism and mirrors gene expression changes reported in breast and lung models exposed to xanthatin or related sesquiterpene lactones (Hsu et al., 2024; Wang et al., 2024). Additionally, inhibition of migration in the scratch assay is consistent with interference in cytoskeletal remodeling and survival signaling, processes in which STAT3 and VEGFR2 are key nodes (Grillo et al., 2025). Methodologically, these anti-migratory effects align with natural product literature using matched scratch assay conditions (Arshad and Saleem, 2025).

Differences between xanthatin and paclitaxel may also reflect pharmacokinetic and resistance properties. Paclitaxel resistance in ovarian cancer is frequently associated with  $\beta$ -tubulin alterations and the activity of drugefflux transporters (Wang et al., 2024). In contrast, in silico ADME predictions in this study indicated that xanthatin is not a substrate for P-glycoprotein and generally exhibits favorable pharmacokinetic properties, which could enhance bioavailability and reduce the risk of resistance (Lee et al., 2025). Moreover, natural product scaffolds such as xanthatin provide tractable templates for analog design-improving solubility or attenuating off-target toxicity—an approach widely employed to translate plant-derived leads toward clinical application (Arshad and Saleem, 2025; Lee et al., 2025).

#### Conclusion

Xanthatin exhibits selective cytotoxicity, ROS-dependent apoptosis, and exerts anti-migratory effects through multi-target protein engagement, distinguishing it from paclitaxel's more limited mechanism of action. These characteristics warrant evaluation in more complex ovarian cancer models, such as spheroids and xenografts, and support testing for synergy with platinum-based agents and PARP inhibitors. Additionally, formulation strategies—such as nanoparticle or micellar delivery systems—may further improve its therapeutic delivery.

# **Financial Support**

Self-funded

## **Ethical Issue**

The guidelines about the development, acquisition, authentication, cryopreservation, and transfer of cell lines between laboratories were strictly followed. Besides, microbial contamination (commonly mycoplasma), characterization, instability, and misidentification was considered seriously.

# **Conflict of Interest**

Authors declare no conflict of interest

# References

Alalawy AI. Key genes and molecular mechanisms related to paclitaxel resistance. Cancer Cell Int. 2024; 24: 244.

Alrosan K, Alrosan AZ, Heilat GB, Alrousan AF, Gammoh OS, Alqudah A, Madaeen S, Alrousan MJ. Treatment of ovarian cancer: From the past to the new era. Oncol Lett. 2025; 30: 384

Arshad H, Saleem M. Cytotoxic effect of *Luffa cylindrica* leaf extract on MCF-7 cell lines. Bangladesh J Pharmacol. 2025; 20: 101-12.

Banerjee P, Eckert AO, Schrey AK, Preissner R. ProTox-II: A webserver for prediction of toxicity of chemicals. Nucleic Acids Res. 2018; 46: W257-63.

Biovia. Discovery Studio Visualizer: User guide. San Diego, CA, Dassault Systèmes BIOVIA, 2021.

BioVision, Inc. Caspase-3 colorimetric assay kit and caspase-9 colorimetric assay kit: Protocols. Milpitas, CA, BioVision, Inc., 2022.

Bustin SA, Benes V, Garson JA, Hellemans J, Huggett J, Kubista M, Mueller R, Nolan T, Pfaffl MW, Shipley GL, Vandesompele J, Wittwer CT. The MIQE guidelines: Minimum information for publication of qPCR experiments. Clin Chem. 2009; 55: 611-22.

Bustin SA, Garson JA, Coward A. The dMIQE guidelines update: Minimum information for digital PCR. Clin Chem. 2020; 66: 1012-29.

Bustin S, Huggett J. qPCR primer design revisited. Biomol Detect Quantif. 2017; 14: 19-28.

Chen H, Zhu T, Huang X, Xu W, Di Z, Ma Y, Xue M, Bi S, Shen Y, Yu Y, Shen Y, Feng L. Xanthatin suppresses proliferation and tumorigenicity of glioma cells through autophagy inhibition via activation of the PI3K-Akt-mTOR pathway. Pharmacol Res Perspect. 2023; 11: e01041.

Chuwa AH, Mvunta DH. Prognostic and clinicopathological significance of surviving in endometrial and ovarian cancers. Oncol Rev. 2024; 13: 1444008.

Daina A, Michielin O, Zoete V. SwissADME: A free web tool to evaluate pharmacokinetics, drug-likeness and medicinal chemistry friendliness of small molecules. Sci Rep. 2017; 7: 42717.

Daina A, Michielin O, Zoete V. SwissTargetPrediction: Updated data and new features for efficient prediction of protein targets of small molecules. Nucleic Acids Res. 2019;

- 47: W357-64.
- Eberhardt J, Santos-Martins D, Tillack AF, Forli S. AutoDock Vina 1.2.0: New docking methods and expanded force field. JCIM. 2021; 61: 3891-98.
- Frąszczak K, Barczynski B. The role of cancer stem cell markers in ovarian cancer. Cancers (Basel). 2024; 16: 40.
- Gao X, Li Y, Xu H, Ni S, Pan H, Ma C, Zhao X, Zhang H. Xanthatin induces apoptosis through ROS-mediated c-FLIP inhibition in human retinoblastoma cells. Front Med. 2025; 12: 1554934.
- Geng Y, Liu P, Xie Y, Liu Y, Zhang X, Hou X, Zhang L. Xanthatin suppresses pancreatic cancer cell growth via the ROS/RBL1 signaling pathway: *In vitro* and *in vivo* insights. Phytomedicine 2023; 119: 155004.
- Grada A, Otero-Vinas M, Prieto-Castrillo F, Obagi Z, Falanga V. Research techniques made simple: analysis of collective cell migration using the wound healing assay. J Invest Dermatol. 2017; 137: e11-16.
- Grillo E, Romani C, Ettorre VM, Santin AD, Mitola S. The VEGF/VEGFR2 system in ovarian cancer: From functional to pharmacological significance. Biochim Biophys Acta Rev Cancer. 2025; 189374.
- He Y, Sun MM, Zhang GG, Yang J, Chen KS, Xu WW, Li B. Targeting PI3K/AKT signal transduction for cancer therapy. Signal Transduct Target Ther. 2021; 6: 425.
- Hsu CY, Rajabi S, Hamzeloo-Moghadam M, Kumar A, Maresca M, Ghildiyal P. Sesquiterpene lactones as emerging biomolecules to cease cancer by targeting apoptosis. Front Pharmacol. 2024; 15: 1371002.
- Izycka N, Rucinski M, Andrzejewska M, Szubert S, Nowak-Markwitz E, Sterzynska K. The prognostic value of cancer stem cell markers (CSCs) expression—ALDH1A1, CD133, CD44—for survival and long-term follow-up of ovarian cancer patients. Prognostic value of ALDH1A1, CD133, CD44 in ovarian cancer. Int J Mol Sci. 2023; 24: 2400.
- Kim S, Chen J, Cheng T, Gindulyte A, He J, He S, Li Q, Shoemaker BA, Thiessen PA, Yu B, Zaslavsky L, Zhang J, Bolton EE. PubChem in 2021: New data content and improved web interfaces. Nucleic Acids Res. 2021; 49: D1388-95.
- Lee E, Yang D, Hong JH. Prominent naturally derived oxidative-stress-targeting drugs and their applications in cancer treatment. Antioxidants. 2025; 14: 49.
- Liang CC, Park AY, Guan JL. In vitro scratch assay: A convenient and inexpensive method for analysis of cell migration in vitro. Nat Protoc. 2007; 2: 329-33.

- Liang ST, Chen C, Chen RX, Li R, Chen WL, Jiang GH, Du LL. Michael acceptor molecules in natural products and their mechanism of action. Front Pharmacol. 2022; 13: 1033003
- Liu Y, Zhang X, Cheng F, Cao W, Geng Y, Chen Z, Wei W, Zhang L. Xanthatin induce DDP-resistance lung cancer cells apoptosis through regulation of GLUT1 mediated ROS accumulation. Drug Dev Res. 2023; 84: 1266-78.
- Livak KJ, Schmittgen TD. Analysis of relative gene expression data using real-time quantitative PCR and the 2- ΔΔCT method. Methods 2001; 25: 402-08.
- Malekzadeh R, Arjmand M, Akbari Z, Sadeghi S, Hosseini RH. The effect of *Xanthium strumarium* root extracts on growth inhibition of epithelial ovarian cancer SK-OV-3 cell line: A metabolomics-based study. Jundishapur J Nat Pharm Prod. 2023; 18.
- Morris GM, Huey R, Lindstrom W, Sanner MF, Belew RK, Goodsell DS, Olson AJ. AutoDock4 and AutoDockTools4: automated docking with selective receptor flexibility. J Comput Chem. 2009; 30: 2785-91.
- Pettersen EF, Goddard TD, Huang CC, Couch GS, Greenblatt DM, Meng EC, Ferrin TE. UCSF Chimera: Visualization system for research and analysis. J Comput Chem. 2004; 25: 1605-12.
- Schindelin J, Arganda-Carreras I, Frise E, Kaynig V, Longair M, Pietzsch T, Preibisch S, Rueden C, Saalfeld S, Schmid B, Tinevez JY. Fiji: An open-source platform for biological-image analysis. Nat Methods. 2012; 9: 676-82.
- Schneider CA, Rasband WS, Eliceiri KW. NIH Image to ImageJ: 25 years of image analysis. Nat Methods. 2012; 9: 671-75.
- Thermo Fisher Scientific. Pierce BCA protein assay kit: User guide. Rockford, IL, Thermo Fisher Scientific, 2022.
- Tia ST, Luo M, Fan W. Mapping the role of P-gp in multidrug resistance: Insights from recent structural studies. Int J Mol Sci. 2025; 26: 4179.
- Tossetta G, Fantone S, Montanari E, Marzioni D, Goteri G. Role of NRF2 in ovarian cancer. Antioxidants 2022; 11: 663.
- van Meerloo J, Kaspers GJ, Cloos J. Cell sensitivity assays: The MTT assay. In: Cancer cell culture: Methods and protocols. Totowa, Humana Press, 2011, pp. 237-45.
- Wang L, Wang X, Zhu X, Zhong L, Jiang Q, Wang Y. Drug resistance in ovarian cancer: From mechanism to clinical application. Mol Cancer. 2024; 23: 66.
- Wordeman L, Vicente JJ. Microtubule targeting agents in disease: Classic drugs, novel roles. Cancers 2021; 13: 5650.

## **Author Info**

Hanzla Arshad (Principal contact) e-mail: hanzlaarshadbutt@gmail.com